High-accuracy maximum power point estimation for photovoltaic arrays

Jen-Cheng Wang [1], Yu-Li Su [1], Jyh-Cherng Shieh, Joe-Air Jiang *

Department of Bio-Industrial Mechatronics Engineering, National Taiwan University, 1, Section 4, Roosevelt Road, Taipei 10617, Taiwan

ABSTRACT

Quantitative information regarding the maximum power point (MPP) of photovoltaic (PV) arrays is crucial for determining and controlling their operation, yet it is difficult to obtain such information through direct measurements. PV arrays exhibit an extremely nonlinear current–voltage (I–V) characteristic that varies with many complex factors related to the individual cells, which makes it difficult to ensure an optimal use of the available solar energy and to achieve maximum power output in real time. Finding ways to obtain the maximum power output in real time under all possible system conditions are indispensable to the development of feasible PV generation systems. The conventional methods for tracking the MPP of PV arrays suffer from a serious problem that the MPP cannot be quickly acquired. Based on the p–n junction semiconductor theory, we develop a prediction method for directly estimating the MPP for power tracking in PV arrays. The proposed method is a new and simple approach with a low calculation burden that takes the resistance effect of the solar cells into consideration. The MPP of PV arrays can be directly determined from an irradiated I–V characteristic curve. The performance of the proposed method is evaluated by examining the characteristics of the MPP of PV arrays depending on both the temperature and irradiation intensity, and the results are discussed in detail. Such performance is also tested using the field data. The experimental results demonstrate that the proposed method helps in the optimization of the MPP control model in PV arrays.

© 2010 Elsevier B.V. All rights reserved.

1. Introduction

In recent years, a critical environmental issue has emerged: how to reduce negative effects brought by global warming and climate change [1–4]. In most cases sources of renewable energy such as the solar energy produced by photovoltaic (PV) arrays should be able to considerably reduce certain carbon dioxide emissions [5,6]. PV arrays are a reliable energy source and an efficient tool for the mitigation of global warming [7,8]. Many countries have initiated energy policies and programs designed to encourage energy diversification, ensure the security of energy supply, facilitate economic efficiency, and improve environmental protection. For example, some governments have introduced policies for the purpose of achieving the goal of energy saving and carbon dioxide reduction. Different approaches are used including encouraging low-energy consumption building designs, installing renewable energy sources, and promoting power management.

Many studies on renewable energy systems have focused on optimizing the use of both PV arrays and conventional energy sources [9–11]. PV arrays have the advantage of directly converting light energy into electrical energy through semiconductors [12,13].

Furthermore, they generate electricity from sunlight instead of using fossil fuels, so no carbon dioxide is emitted. Nor do they require turbines and cooling water during operation. In addition, PV arrays are highly reliable and easy to use. PV energy has attracted intensive research efforts in recent years due to its unique properties and versatile applications [14–16]. However, the energy-conversion efficiency of such arrays is still low. Hence, more attention needs to be paid to ways to improve the performance of PV arrays and to further investigate energy conversion processes and energy loss issues related to their use.

The photovoltaic modules of the PV generation system convert solar energy into direct current (dc) electricity. However, the PV arrays exhibit the characteristic of an extremely nonlinear current–voltage (I–V) which varies with array temperature and solar irradiation over time which complicates the locating of the MPP. Many complex factors, such as temperature, aging, and the possible breakdown of individual cells, may also influence PV arrays, making it difficult to ensure the optimal use of the available solar energy to achieve maximum power output in real time under all possible system operation conditions [17,18]. A maximum power point tracking (MPPT) control method is required to ensure that the PV generation system achieves the maximum power output in real time. Various methods, such as the lookup table method [17,18], perturb-and-observe method [19–22], and incremental conductance method [23,24], have been proposed when applying the MPPT algorithm to PV arrays to ensure maximum utilization

efficiency. These functions are usually implemented or controlled by the circuits. Almost all such circuits act as interfaces between the PV generators and the loads or energy accumulators, in most cases operating in off-line mode. Due to the complexity of the mathematical operations involved in the afore-mentioned methods, a digital signal processor or a relatively powerful microcontroller is typically needed to implement them. This increases the cost of the power processing circuit. Clearly, a less complicated way of tracking the MPP through a convenient estimation technique is required.

Aside from the shortcomings mentioned above, it is impossible for the conventional methods to quickly acquire the MPPs for the power generated by PV arrays. This means that the tracking of the maximum power output of PV arrays cannot be achieved in real time. To facilitate the efficiency of the MPPT algorithm, a new, simple, and direct-prediction method with a low calculation burden is introduced in this study. This method is developed based on the p–n junction semiconductor theory of solar cells. Both the temperature and irradiation intensity characteristics of the MPP of PV arrays are taken into account. The proposed direct-prediction method is not only able to decrease tracking time and energy loss, but also increase power utilization.

The rest of this paper is organized as follows: Section 2 describes the theoretical details of the proposed method and emphasizes its features. Section 3 presents the experimental procedures and describes the material of the PV arrays and the test conditions for various irradiation situations. The experimental results yielded by the numerical simulation and field-test data are reported in Section 4. Finally, the conclusions are given in the last section.

2. Theoretical basis of the proposed method

PV arrays are known to be nonlinear, with one operating point existing where the PV array produces the maximum power. The nonlinear temperature-dependent behaviors of PV arrays have been successfully described by the p–n junction recombination mechanism of semiconductors [25]. In order to achieve maximum utilization efficiency, we develop a simplified method to directly estimate the MPP by using the p–n junction semiconductor theory.

Fig. 1 depicts the equivalent circuit of the PV array. Based on the p–n junction recombination mechanism, the output current I of a solar array is given by Eq. (1) using the symbols shown in Fig. 1 [25–27], i.e.

$$I = I_g - I_d - V_d/R_{sh}, \tag{1}$$

where I_g is the light-generated photocurrent (A); R_{sh} the parallel resistance (ohm); I_d and V_d the current and voltage of the p–n junction diode. The current I_d and voltage V_d of the p–n junction diode are given by

$$V_d = V + IR_s, \tag{2}$$
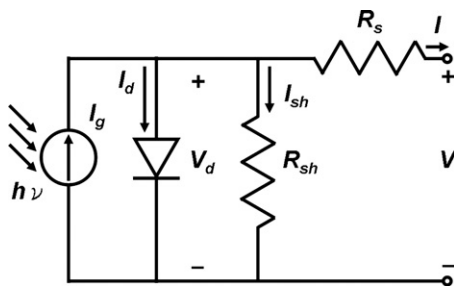

Fig. 1. The equivalent circuit for PV arrays.

and

$$I_d = I_{sat} \left\{ \exp\left[\frac{qV_d}{nkT}\right] - 1 \right\}, \tag{3}$$

where R_s is the series resistance (ohm); I_{sat} the reverse saturation current (A); n the ideality factor of the diode; q the electron charge (C); k Boltzmann's constant (eV K^{-1}); and T the temperature (K). The ideality factor (n) of the diode is usually set as 1 when only the diffusion current flows across the junction and 2 when the recombination current dominates [25]. Thus, the ideality factor of the diode could be considered as a constant and independent of voltage [25]. A series resistance can be caused either by excessive contact resistance or the resistance of the neutral regions. The series resistance R_s accounts for all voltage drops across the transport resistance of the solar cell, and R_s connects to a load or an inverter. The series resistance (R_s) can be determined by various methods under various illumination conditions, such as dark, constant illumination, and varying illumination [28]. In the standardized measurement methods for solar cells, R_s is normally determined from two different illumination levels, the so-called two-curve method [29].

The parallel resistance (R_{sh}) usually results from any channel that bypasses the p–n junction. This bypass can be brought about by damaged regions on the p–n junction or surface imperfections. The parallel resistance R_{sh}, in parallel with the diode of the solar cell model, represents the shunt paths which can occur in real solar cells across the surface, at pin holes in the p–n junction, or at grain boundaries. The parallel resistance (R_{sh}) can be obtained from only one illuminated I–V curve, the single curve method. Both R_s and R_{sh} are independent of the illumination level and the operating voltage [30].

After substituting the components related to the p–n junction diode into Eq. (1), the output current I (i.e., the current I_{pv} of PV arrays) can be expressed by [25–27]

$$I = I_{pv} = I_g - I_{sat}\left\{\exp\left[\frac{q(V_{pv} + I_{pv}R_s)}{nkT}\right] - 1\right\} - \frac{V_{pv} + I_{pv}R_s}{R_{sh}}. \tag{4}$$

When the PV arrays connect to the load, the circuit parameters of PV arrays I and V become I_{pv} and V_{pv}. The terms related to the parallel resistance R_{sh} can be generally ignored, because the parallel resistance of PV arrays is relatively high in the majority of practical cases, and Eq. (4) is further simplified to

$$I_{pv} = I_g - I_{sat}\left\{\exp\left[\frac{q(V_{pv} + I_{pv}R_s)}{nkT}\right] - 1\right\}. \tag{5}$$

The power generated from the PV arrays is

$$P_{pv} = I_{pv}V_{pv}. \tag{6}$$

The power slope β with respect to the voltage variation of PV arrays can be expressed as [31]

$$\beta = \frac{dP_{pv}}{dV_{pv}} = I_{pv} + \frac{dI_{pv}}{dV_{pv}}V_{pv}$$

$$= I_g - I_{sat}\left\{\exp\left[\frac{q(V_{pv} + I_{pv}R_s)}{nkT}\right] - 1\right\}$$

$$- \frac{qI_{sat}}{nkT}\exp\left[\frac{q(V_{pv} + I_{pv}R_s)}{nkT}\right]\left(1 + \frac{dI_{pv}}{dV_{pv}}R_s\right)V_{pv}. \tag{7}$$

The maximum utilization efficiency and maximum power are achieved when the power slope $\beta = 0$, and Eq. (7) can be further simplified to

$$I_g + I_{sat} = I_{sat}\exp\left[\frac{q(V_{mp} + I_{mp}R_s)}{nkT}\right]\left(1 + \frac{qV_{mp}}{nkT} + \frac{qV_{mp}R_s}{nkT}\frac{dI_{pv}}{dV_{pv}}\bigg|_{V_{pv} = V_{mp}}\right) \tag{8}$$

or

$$\frac{I_g + I_{sat}}{I_{sat}} = \exp\left[\frac{q(V_{mp} + I_{mp}R_s)}{nkT}\right]\left(1 + \frac{qV_{mp}}{nkT} + \frac{qV_{mp}R_s}{nkT} \cdot \frac{dI_{pv}}{dV_{pv}}\bigg|_{V_{pv} = V_{mp}}\right),$$

$$(9)$$

where I_{mp} and V_{mp} represent the current and voltage of PV arrays operated in the maximum power output mode. On the other hand, the output current I is zero when the load disconnects, and the open-circuit voltage V_{oc} can be calculated by [32]

$$\frac{I_g + I_{sat}}{I_{sat}} = \exp\left[\frac{qV_{oc}}{nkT}\right],$$

$$(10)$$

or

$$V_{oc} = \frac{nkT}{q}\ln\left[\frac{I_g + I_{sat}}{I_{sat}}\right].$$

$$(11)$$

The light-generated photocurrent I_g and the reverse saturation current I_{sat} of PV arrays are obtained from a standard test condition. From Eqs. (9) and (10), we can obtain the characteristic equation that represents the operation of PV arrays at the MPP, which can be expressed by

$$1 + \frac{qV_{mp}}{nkT} + \frac{qV_{mp}R_s}{nkT}\frac{dI_{pv}}{dV_{pv}}\bigg|_{V_{pv} = V_{mp}} = \exp\left[\frac{q}{nkT}(V_{oc} - V_{mp} - I_{mp}R_s)\right]. \quad (12)$$

For a parallel-connected PV power conditioning system with a line connection, the effective line power P_s can be written as [31]

$$P_s = V_S I_S \cos\theta = V_S I_T,$$

$$(13)$$

where V_S is the root-mean-square (rms) value of the line voltage (V); I_S the rms value of the line current (A); θ the angle of the line current (radians); and $I_T = I_S \cos\theta$ the rms value of the line current (A). On the other hand, the dc power P_{pv} generated from the PV arrays is calculated by

$$P_{pv} = I_{pv}V_{pv}.$$

$$(14)$$

From the law of power conservation, the generated dc power P_{pv}, considering the power conservation efficiency, should be equal to the effective line power such that

$$\eta P_{pv} = P_s,$$

$$(15)$$

where η is the power conservation efficiency of the generated dc power P_{pv} compared with the effective line power P_s. In general, the power conservation efficiency η can reach up to 99% with a parallel-connected PV power conditioning system with a line connection [31]. Hence, the power conservation efficiency η will be considered as constant in this work. From Eqs. (13) to (15), the dc current I_{pv} of the PV arrays can be estimated as

$$I_{pv} = \frac{V_S I_T}{\eta V_{pv}}.$$

$$(16)$$

Thus, the current I_{pv} of the PV arrays can be estimated without directly using a dc current sensor. In general, the dc current sensor requires additional positive and negative voltage sources. Moreover, a dc current sensor is expensive compared to an ac current sensor, and makes the overall system more complex [31]. Combining Eq. (12) with Eq. (16) gives

$$1 + \frac{q}{nkT}V_{mp} - \frac{q}{nkT}\left(\frac{V_S I_T}{\eta V_{mp}}\right)R_s = \exp\left[\frac{q}{nkT}\left(V_{oc} - V_{mp} - \frac{V_S I_T}{\eta V_{mp}}R_s\right)\right].$$

$$(17)$$

In practical applications of the PV arrays, the open-circuit voltage V_{oc} is usually given or measurable under standard test conditions. From the experimental results, we find that the voltage V_{mp} of PV arrays operated at the MPP is near linearly proportional to the open-circuit voltage V_{oc} of PV arrays operated under various

environmental conditions, i.e., varying irradiation intensities and temperatures. One finding is that the V_{mp}/V_{oc} characteristic remains almost constant as the irradiation intensity increases. On the other hand, the V_{oc} and V_{mp} of the PV arrays both decrease linearly with the increase of temperature.

In order to directly estimate the MPP based on the afore-mentioned findings, we suppose that the voltage V_{mp} at the MPP can be expressed as proportional to the open-circuit voltage V_{oc}, specifically

$$V_{mp} = mV_{oc}.$$

$$(18)$$

Since the parameters that appear in Eq. (17) are either related to the semiconductor fabrication process or to on-line measurable ones, the value of V_{mp} can be calculated from Eq. (17) directly. Then, using the m value calculated from Eq. (18), we can directly obtain the MPP of PV arrays in real time. This is done by incorporating the irradiated I–V characteristic curve and the fabrication process parameters of PV arrays even if the irradiation conditions are changed. This m index provides necessary information about the MPP of the PV arrays and can be used to track the location of the MPP in practical applications. The validity of Eq. (18) with respect to various operating conditions will be demonstrated using the field-test data and discussed in Section 4.

When we apply the proposed direct-prediction method to a parallel-connected PV power conditioning system, Eq. (17) can be modified, substituting the assumption of Eq. (18) into Eq. (17), and yields

$$1 + \frac{q}{nkT}mV_{oc} - \frac{q}{nkT}\left(\frac{V_S I_T}{\eta mV_{oc}}\right)R_s = \exp\left[\frac{q}{nkT}\left(V_{oc} - mV_{oc} - \frac{V_S I_T}{\eta mV_{oc}}R_s\right)\right],$$

$$(19)$$

where q and k are the constants; n the ideality factor of the diode; and T the temperature. The characteristic parameters of the PV arrays, V_{oc} and R_s, are dependent on the semiconductor fabrication process and the different weather conditions, and both can be obtained from the data sheets for the PV arrays. On the other hand, the effective line power $P_s = V_S I_T$ and the power conservation efficiency η are given for the parallel-connected PV power conditioning system with a line connection. In general, the power conservation efficiency η can be as high as 99% for the parallel-connected PV power conditioning system with a line connection [31]. Hence, in this work the power conservation efficiency η will be considered as constant and we set $\eta = 99\%$. Therefore, from Eq. (19), we can directly evaluate the m value and then estimate the V_{mp} at the MPP of the PV arrays by using Eq. (18).

Subsequently, we develop a method to estimate the current and the output power of PV arrays operating at the MPP. When the output voltage V is zero, the short-circuit current I_{sc} is given by [33]

$$I_{sc} = I_g - I_{sat}\left\{\exp\left[\frac{q(I_{sc}R_s)}{nkT}\right] - 1\right\},$$

$$(20)$$

and the current I_{mp} at the MPP is given by

$$I_{mp} = I_g - I_{sat}\left\{\exp\left[\frac{q(V_{mp} + I_{mp}R_s)}{nkT}\right] - 1\right\}$$

$$= I_{sc} + I_{sat}\exp\left[\frac{q(I_{sc}R_s)}{nkT}\right] - I_{sat}\exp\left[\frac{q(V_{mp} + I_{mp}R_s)}{nkT}\right].$$

$$(21)$$

Substituting Eqs. (10) and (20) into Eq. (21), I_{mp} is expressed by

$$I_{mp} = I_{sc}\left[1 - \exp\left[\frac{q(V_{mp} - V_{oc})}{nkT}\right]\exp\left[\frac{q(I_{mp}R_s)}{nkT}\right]\right]$$

$$(22)$$

or

$$\ln\left(1 - \frac{I_{mp}}{I_{sc}}\right) = \frac{q}{nkT}(V_{mp} - V_{oc} + I_{mp}R_s).$$

$$(23)$$

The ideality factor of the diode, which is defined as n, can be calculated by Eq. (11). This means that with Eq. (23) we can convert I_{mp} into a measurable quantity. Thus, using Eqs. (11) and (20), the

output voltage V_{pv} can be described as a function of the output current I_{pv} with the circuit parameters V_{oc}, I_{sc}, V_{mp}, and I_{mp} given in the following equation as:

$$V_{pv} = V_{oc}\left[1 - \frac{I_{pv}R_s}{V_{oc}} + \left[\left(\frac{V_{mp}}{V_{oc}} - 1 + \frac{I_{mp}R_s}{V_{oc}}\right)\frac{1}{\ln(1-I_{mp}/I_{sc})}\right]\ln\left(1 - \frac{I_{pv}}{I_{sc}}\right)\right].$$
(24)

Finally, the output power P_{pv} generated from the PV arrays is expressed as a function of the output current I_{pv} and the output voltage V_{pv}. Then, the P–I characteristics of PV arrays can be calculated by

$$P_{pv} = V_{pv} \times I_{pv}$$
$$= I_{pv} \times V_{oc}\left[1 - \frac{I_{pv}R_s}{V_{oc}} + \left[\left(\frac{V_{mp}}{V_{oc}} - 1 + \frac{I_{mp}R_s}{V_{oc}}\right)\frac{1}{\ln(1-I_{mp}/I_{sc})}\right]\ln\left(1 - \frac{I_{pv}}{I_{sc}}\right)\right].$$
(25)

The values of V_{oc}, I_{sc}, and R_s are obtained from the data sheets for the PV arrays, while the values of V_{mp} and I_{mp} are measured under various situations, such as different combinations of irradiation intensities and temperatures.

In summary, it is easy to estimate the MPP and output of PV arrays using our prediction method based on the p–n junction recombination mechanism. This ensures that maximum utilization efficiency and maximum power are achieved in practical applications. The proposed method is a new and simple approach with a low calculation burden, which can be used to directly determine the MPP of PV arrays from an irradiated I–V characteristic curve. This direct-prediction method could be further applied to the MPPT algorithm for any kind of PV arrays. It is expected that using the proposed method we can achieve a maximum power output in real time and substantially increase the output power of PV arrays in a solar generation system.

3. Experimental procedure

The output current and voltage of PV arrays are directly affected by many factors such as the resistance, illuminance, and temperature. In this study, we develop a prediction method for directly estimating the MPP of PV arrays which takes the resistance effect of the solar cells into consideration. The temperature-dependent and irradiation intensity-dependent characteristics of the MPP of PV arrays are used to evaluate the performance of the proposed method, and the results are discussed in detail. We also conduct experiments, including both numerical simulation and field data tests, to evaluate the performance of the proposed direct-prediction method.

Due to the difficulties of real-world experimental set-up, the experiments with respect to resistance effects of the solar cells were only performed by numerical simulation. The goal was to show that the proposed method can be used to directly determine the MPP of PV arrays from an irradiated I–V characteristic curve, even under various resistance effects. The light-generated photocurrent and the reverse saturation current of PV arrays are assumed to be $I_g=100$ mA and $I_{sat}=1$ nA [25], respectively. The ideality factor of the diode (n) is set as $n=1$. The impact of varying resistances on the fill factor (FF) [25] of PV arrays is also discussed in detail.

Both temperature-dependent and irradiation intensity-dependent characteristics of the MPP of PV arrays were considered in the field data tests. A PV array comprised of 60 commercial cells connected in series was used in the field tests. The generated data was used to evaluate the performance of the proposed direct-prediction method. The size of each cell was 35×50 mm^2. P-type, multi-crystalline silicon (mc-Si) wafers with a resistivity of around

0.5–3 Ω cm were used in these experiments. The I–V characteristics of the PV arrays were measured under standard test conditions; irradiation intensity of 1000 W/m^2; AM 1.5 G; and temperature of 25 °C. Both the temperature and irradiation intensity were taken into account. The characteristics of the PV arrays under different illumination levels and temperatures were also examined using a solar simulator (SPI-SUN SIMULATOR 4600, Spire). The experiments for field data tests were conducted at three illumination levels; 600, 800, and 1000 W/m^2 and four temperatures; i.e., 0, 25, 50, and 75 °C. Field test data were obtained under different illumination levels and temperatures for the same ten PV arrays. The measurement of the I–V characteristics was repeated 100 times. The assumptions for the m values under various operation conditions were also verified and discussed in detail.

4. Results and discussion

4.1. Basic performance evaluation with respect to the resistance effect

In this subsection, the current–voltage characteristic of a single solar cell with different series resistances under constant irradiation intensity is examined. In this numerical simulation, the p–n junction parameters of the single solar cell are set as $I_g=100$ mA and $I_{sat}=1$ nA [25]. The forward current in a p–n junction is dominated by the recombination of the minority carriers injected into the neutral regions of the junction. This type of the current gives an ideality factor (n) of 1.0 [25]. The recombination of the carriers in the space charge region results in an ideality factor (n) of 2.0 [25]. Normally, the PV cell or PV models adopted by the crystalline silicon PV modules have an ideality factor of between 1 and 2. Nevertheless, different studies have shown that $n=1$ is adequate for modeling purposes [34]. The ideality factor of the diode will be thus taken as $n=1$ in this simulation.

The mathematical simulation results when $I_g=100$ mA, $I_{sat}=1$ nA, and $T=300$ K, under different R_s values ($R_s=0$, 1, 3, and 5 Ω), are depicted in Fig. 2(a). An inspection of Fig. 2(a) indicates that the open-circuit voltage V_{oc} and short-circuit current I_{sc} of the single solar cell with $R_s=0$ Ω are 0.47 V and 100 mA, respectively. It is worth noting that many factors degrade the ideal power efficiency. One of the major factors is the series resistance R_s that originates from ohmic loss from the front surface of the PV cell or array. The output voltage of the single solar cell decreases linearly to the current when the series resistance increases. On the other hand, the output current of the single solar cell decreases inversely proportional to the voltage under decreasing parallel resistance. Both effects, separately and together, lead to a smaller fill factor (FF) which is expressed as $FF=(I_{mp}V_{mp})/(I_{sc}V_{oc})=P_{mp}/(I_{sc}V_{oc})$ [25]. The maximum power of the single solar cell with different R_s values ($R_s=0$, 1, 3, and 5 Ω) calculated by Eqs. (17) and (22) are 37.7, 29.2, 16.3, and 10.5 mW, respectively, as indicated by the arrows in Fig. 2(b). The open-circuit voltages (V_{oc}) of the single solar cell with different R_s are almost constant at 0.47 V, as indicated in Fig. 2(a). The corresponding short-circuit currents (I_{sc}) of the single solar cell calculated by Eq. (20) are 100, 100, 100, and 85 mA for $R_s=0$, 1, 3, and 5 Ω, respectively. Clearly, the fill factors of a single solar cell decrease from 80.2% to 22.3% with an increase in the series resistance R_s from 0 to 5 Ω.

Fig. 2(b) shows the power–voltage curve of a single solar cell with different series resistances under constant irradiation intensity. By substituting the related parameters into Eqs. (11), (18), and (19) of the direct-prediction method, the MPP of the single solar cell for each series resistance can be estimated, as indicated by the labeled arrows in Fig. 2(b). The average difference and mean error between the simulated and estimated voltages for a single solar cell operating at MPP are 0.02 V and 0.5%, respectively.
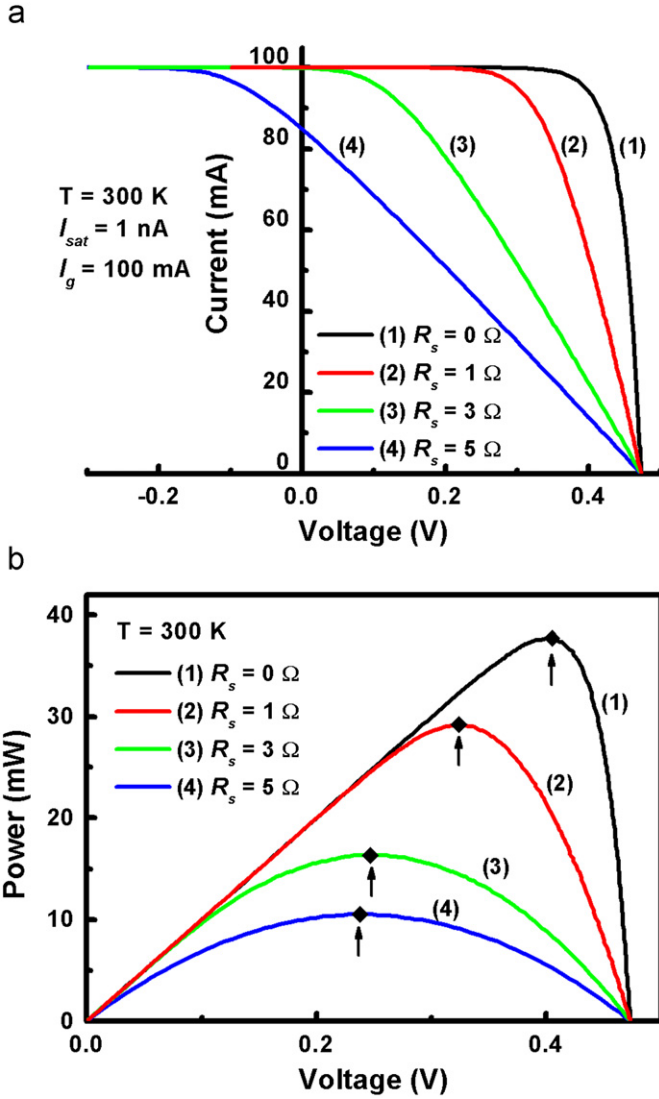
a

b

Fig. 2. Numerical simulation results. (a) The current–voltage characteristic of the PV arrays with different series resistance under a constant irradiation intensity. (b) The power–voltage curve of the PV arrays with different series resistances under a constant irradiation intensity. The labeled arrows indicate the MPP of the PV arrays with different series resistances estimated by the direct-prediction method.

The maximum power outputs with respect to two different series resistances R_s of 0 and 5 Ω are 100% and 25.3%, respectively. This implies that a series resistance of 5 Ω yields a 74.7% reduction in the maximum power when $R_s=0$. These experiments show that the method presented here is accurate and simple to calculate. This is an effective way to determine the MPP of PV arrays from a single irradiated I–V characteristic curve taking the resistance effect into consideration. The experimental results also demonstrate that the resistance has a critical effect on the characteristic of the PV arrays.

4.2. Performance evaluation for various irradiation intensities

Fig. 3 shows the I–V–P (current–voltage–power) curves of PV arrays at 25 °C subject to different irradiation intensities. The symbols indicate the MPPs for different irradiation intensities estimated by the direct-prediction method. The open-circuit

voltage V_{oc} and the short-circuit current I_{sc} of the PV arrays are 36.83 V and 7.86 A, as measured under standard test conditions; irradiation intensity of 1000 W/m^2; AM 1.5 G; and temperature of 25 °C. The PV arrays used in the experiment are constructed of 60 serially connected cells. The area of each cell is equal to 1.623 m^2 with $R_s=0.006$ Ω and $R_{sh}=10^4$ Ω. The light-generated photocurrent I_g and the reverse saturation current I_{sat} obtained for the PV arrays under standard conditions are 7.94 A and 13.7 μA. As mentioned above, the power conservation efficiency η for the parallel-connected PV power conditioning system with line connection is set at $\eta=99\%$. As described in Section 2, the ideality factor n of the diode can be calculated by Eq. (11). This suggests that Eq. (11) can convert n into a measurable quantity. Through Eq. (11), we can calculate the ideality factor of the PV cell to be $n=1.8$, using the parameters mentioned above. The n value lies reasonably between the expected values for the diffusion and generation recombination mechanisms [25]. Furthermore, we also want to investigate the effects of the various irradiation intensities on the I–V curve of PV arrays.

Table 1 summarizes the irradiation intensity dependence of the V_{oc}, V_{mp}, and V_{mp}/V_{oc} for the PV arrays at a temperature of 25 °C. In addition, two prediction performance indices are used to measure the prediction performance of the proposed method, and they are defined as follows: (1) Prediction error in V_{mp}: $\Delta V_{mp}=V_{mp\text{(direct-prediction}}$ $_\text{method)}-V_{mp\text{(Experimental results)}}$ and (2) Percentage prediction error in V_{mp}/V_{oc}: $V_{mp}/V_{oc}(\%)=[(V_{mp}/V_{oc\text{(direct-prediction method)}}-V_{mp}/V_{oc\text{(Experimental results)}})/(V_{mp}/V_{oc\text{(Experimental results)}})]\times 100\%$. The test results for these two performance indices are also included in Table 1. It can be seen that the values of the open-circuit voltage V_{oc} and the voltage V_{mp} at the MPP rise due to the increase in the irradiation intensity, but the values of the V_{mp}/V_{oc} ratios remain almost the same at 0.8144, being insensitive to the changes of the irradiation intensity. Using the direct-predication model to estimate the value of V_{mp} and the ratios of V_{mp}/V_{oc}, we obtain the same tendency for the irradiation intensity-dependent variation of the values of V_{oc} and V_{mp} and the high-accuracy estimation at the MPP for photovoltaic arrays. Furthermore, with the rise in the irradiation intensity, an increase in the output power as indicated by the symbols in Fig. 3 is primarily caused by the rise in the open-circuit voltage V_{oc} giving rise to a linear increase in the photocurrent. The average values of the prediction error ΔV_{mp} and the percentage prediction error $V_{mp}/V_{oc}(\%)$ for the actual and estimated maximum power voltages of the PV arrays are 0.025 V and 0.08%, respectively. This confirms that the voltage V_{mp} at the MPP of the PV
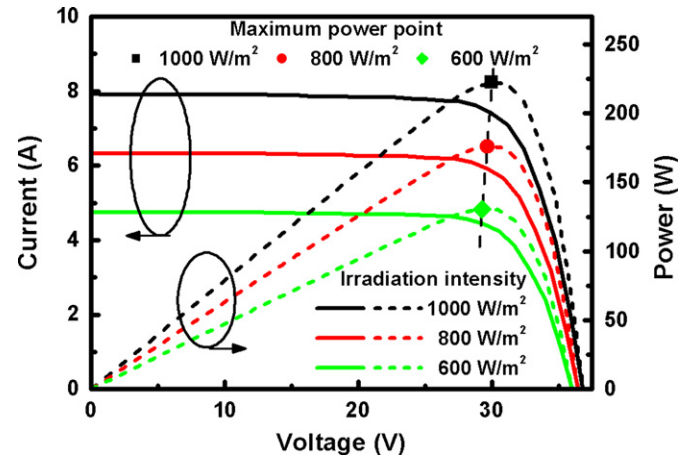

Fig. 3. The current–voltage–power characteristic of the PV arrays under different irradiation intensities and temperature of 25 °C. The labeled arrows indicate the MPPs of the PV arrays with different irradiation intensities estimated by the direct-prediction method.

Table 1
The dependence of the V_{oc}, V_{mp}, V_{mp}/V_{oc}, and two prediction performance indices for the PV arrays on different irradiation intensities under temperature of 25 °C. The test results were experimentally measured and estimated by the direct-prediction method, respectively.

Irradiation intensity (W/m²)	Experimental results			Direct-prediction method		Prediction performance indices	
	V_{oc} (V)	V_{mp} (V)	V_{mp}/V_{oc}	V_{mp} (V)	V_{mp}/V_{oc}[a]	Prediction error: ΔV_{mp} (V)	% Prediction error: V_{mp}/V_{oc}
1000	36.828	29.991	0.8144	30.015	0.8150	0.024	0.07
800	36.459	29.692	0.8144	29.678	0.8139	−0.019	−0.06
600	36.018	29.334	0.8144	29.312	0.8135	−0.033	−0.11

[a] The values of open-circuit voltage (V_{oc}) used are the same as the experimental ones.

Table 2
The dependence of the I_{sc}, I_{mp}, I_{mp}/I_{sc}, and two prediction performance indices for the PV arrays on different irradiation intensities under temperature of 25 °C. The test results were experimentally measured and estimated by the direct-prediction method, respectively.

Irradiation intensity (W/m²)	Experimental results			Direct-prediction method		Prediction performance indices	
	I_{sc} (A)	I_{mp} (A)	I_{mp}/I_{sc}	I_{mp} (A)	I_{mp}/I_{sc}[a]	Prediction error: ΔI_{mp} (A)	% Prediction error: I_{mp}/I_{sc}
1000	7.938	7.409	0.9334	7.402	0.9325	−0.007	−0.10
800	6.351	5.927	0.9332	5.921	0.9336	0.002	0.04
600	4.763	4.448	0.9338	4.451	0.9344	0.003	0.06

[a] The values of short-circuit current (I_{sc}) used are the same as the experimental ones.

arrays can be simply and accurately estimated using the direct-prediction method.

Experiments were also conducted with three irradiation intensities under the same temperature of 25 °C. The test results for irradiation intensity dependence on the I_{sc}, I_{mp}, and I_{mp}/I_{sc} of the PV arrays are listed in Table 2. Similarly, two performance indices are used to measure the I_{mp} prediction performance of the proposed method, and they are defined as follows: (1) Prediction error in I_{mp}: $\Delta I_{mp} = I_{mp(\text{direct-prediction method})} - I_{mp(\text{Experimental results})}$ and (2) Percentage prediction error in I_{mp}/I_{sc}: $I_{mp}/I_{sc}(\%) = [(I_{mp}/I_{sc(\text{direct-prediction method})} - I_{mp}/I_{sc(\text{Experimental results})})/(I_{mp}/I_{sc(\text{Experimental results})})] \times 100\%$. From Table 2, it can be clearly seen that the current I_{mp} of the MPP is proportional to the maximum power when maintaining the solar panels at a constant temperature. Furthermore, the values of the short-circuit current I_{sc}, the current I_{mp} of the MPP, and the ratio of I_{mp}/I_{sc} are all correlated with irradiation intensity levels. The short-circuit current I_{sc} increases linearly from 4.763 to 7.938 A with the minority carrier concentration due to the increase in the irradiation intensity. However, it is found that the ratios of I_{mp}/I_{sc} stay near the average value of 0.9335, being insensitive to changes of the irradiation intensity. The average values of the prediction error ΔI_{mp} and the percentage prediction error I_{mp}/I_{sc} (%) between the actual and estimated maximum power currents of the PV arrays are 0.004 A and 0.063%, respectively. The data indicates that the estimations of I_{mp} and I_{mp}/I_{sc} obtained using the proposed direct-prediction method are very accurate with little error.

Fig. 4 shows plots of the P–I characteristic curves for the PV arrays calculated using Eq. (25) for the experimental data under different irradiation intensities and the temperature of 25 °C. The hollow symbols and dashed lines in Fig. 4 indicate the experimental and calculated P–I characteristic curves, respectively. The labeled solid symbols in Fig. 4 indicate the MPPs of the PV arrays obtained under different irradiation intensities. Using Eqs. (19) and (23), these MPPs are calculated from the values of V_{mp}, V_{oc}, I_{mp}, and I_{sc}, which are acquired from Fig. 3. This is also verified through the experimental results shown in Fig. 4. The comparison of the calculated results with the experimental results in Fig. 4 shows that both are pretty similar. These experimental results verify that
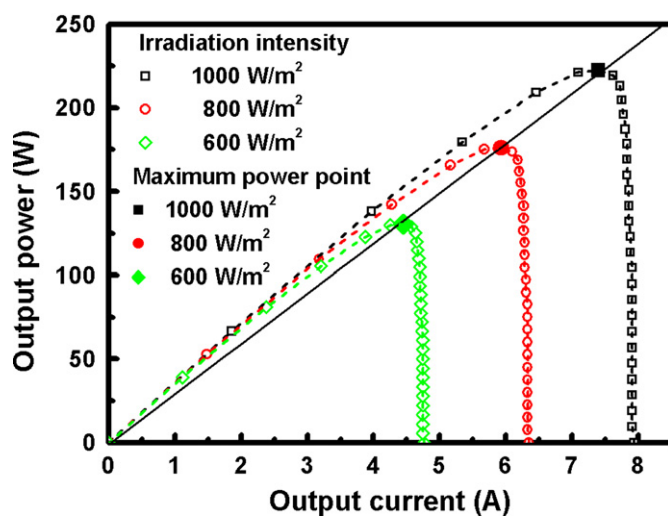

Fig. 4. The experimental and calculated P–I characteristics curves of the PV arrays under different irradiation intensities and temperature of 25 °C. The hollow symbols and dash lines in figure indicate the experimental and calculated P–I characteristics curves of the PV arrays, respectively. The labeled solid symbols indicate the MPPs of the PV arrays with different irradiation intensities estimated by the direct-prediction method.

the maximum power currents of the PV arrays can also be accurately estimated with the proposed direct-prediction method.

As noted above the MPP of the PV arrays and the value of m (i.e., V_{mp}/V_{oc}) can be directly estimated. Furthermore, by substituting the values of V_{mp} and V_{oc} into Eq. (23), we can also directly estimate the ratio of I_{mp} to I_{sc}. Variations in the ratios V_{mp}/V_{oc} and I_{mp}/I_{sc} are shown in Fig. 5 and listed in Tables 1 and 2, respectively. The dashed lines in Fig. 5 indicate the results obtained by applying linear least square fitting to the experimental data for different irradiation intensities. As the irradiation intensity increases, the ratios V_{mp}/V_{oc} and I_{mp}/I_{sc} remain almost constant. These facts are important for finding the operation characteristics of PV arrays. Moreover, it is

confirmed that there is also a proportional relationship between the short-circuit current I_{sc} and the current I_{mp} of the MPP determined by Eq. (22), as shown by the dashed lines in the inset to Fig. 5. Based on the empirical rule, the ratio I_{mp}/I_{sc} is 0.9 [33]. On the other hand, the inset of Fig. 5 also shows that the linear proportionality relationship between the short-circuit current I_{sc} and the current I_{mp} of the MPP is almost constant and equal to 0.933, which is more accurate than the empirically current
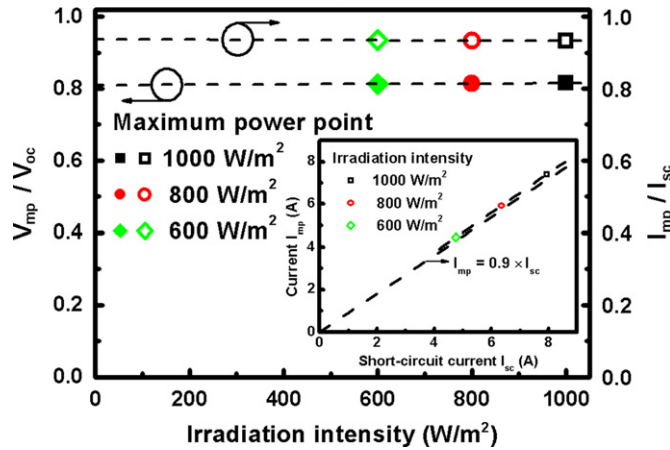
proportion of I_{mp}/I_{sc}, even if the irradiation intensity is changed. The short-circuit current increases linearly in line with the light-generated carrier concentration, and the open-circuit voltage increases at a rate of 0.1 V per decade of irradiation intensity, while the fill factor degrades slightly [25]. This increase is primarily the result of the increase in V_{oc}. Similarly, the photocurrent I_g increases linearly with the growth in the irradiation intensity and the current I_{mp} of the MPP is proportional to the irradiation.

Fig. 5. The characteristic ratios of V_{mp}/V_{oc} and I_{mp}/I_{sc} estimated from the $P–I$ characteristic curve of the PV arrays under different irradiation intensities and temperature of 25 °C. The inset shows the relationship between the short-circuit current I_{sc} and the current I_{mp} at the MPP for the PV arrays under different irradiation intensities and temperature of 25 °C.
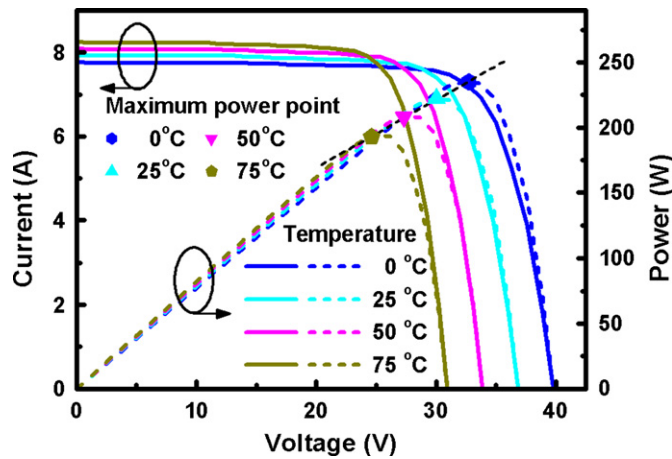
4.3. Performance evaluation versus temperature

The $I–V–P$ (current–voltage–power) curves of the PV arrays under different temperatures and an irradiation intensity of 1000 W/m^2 are depicted in Fig. 6. The symbols shown in Fig. 6 indicate the MPPs of PV arrays operated under different temperatures, which are estimated by the direct-prediction method. Examining the figure one observes that the performance of the PV arrays is affected by the temperature, with the voltage of the PV arrays decreasing as the temperature climbs. The decrease in temperature depends on the open circuit voltage and the band gap of the semiconductor material used to make the PV cell. From Figs. 3 and 6, it can be observed that the changes in irradiation mainly affect the PV output current, while the temperature changes mainly influence the PV output voltage. As the device temperature goes up, V_{oc} will rapidly decline due to the exponential dependence of the saturation current I_{sat} on temperature while I_{sc} slightly increases.

Table 3 shows the temperature dependence of the V_{oc}, V_{mp}, and V_{mp}/V_{oc} for PV arrays under an irradiation intensity of 1000 W/m^2. The temperature effects on the two performance indices (the prediction error ΔV_{mp} (V) and the percentage prediction error V_{mp}/V_{oc} (%)) are also summarized in Table 3. When the device temperature rises, it leads not only to a rapid decrease in the V_{oc} from 39.774 to 30.936, but also to a decrease in the ratio of V_{mp}/V_{oc}. The average values of the prediction error ΔV_{mp} and the percentage prediction error V_{mp}/V_{oc} (%) for the PV arrays are 0.169 V and 0.61%, respectively. The small prediction error and percentage prediction error for the voltage at MPP of the PV arrays indicate that the proposed method provides pretty good prediction performance.

Fig. 7 shows the $P–I$ characteristic curves of the PV arrays plotted in relation to the experimental data and as calculated by Eq. (25). In this test case, different temperatures are used while the irradiation intensity is set at 1000 W/m^2. The hollow symbols and dashed lines indicate the experimental and calculated $P–I$ characteristic curves. The labeled solid symbols in Fig. 7 indicate the MPPs of the PV arrays under different temperatures. Using Eqs. (19) and (23) we calculate the MPPs from the values acquired from Fig. 6.

The temperature dependence of the I_{sc}, I_{mp}, and I_{mp}/I_{sc} for the PV arrays under an irradiation intensity of 1000 W/m^2 is summarized in Table 4. As the device temperature begins to raise, the diffusion lengths increase, and the minority-carrier lifetimes also increase.

Fig. 6. The current–voltage–power characteristic of the PV arrays under different temperatures and an irradiation intensity of 1000 W/m^2. The labeled arrows indicate the MPPs of the PV arrays with different temperatures estimated by the direct-prediction method.

Table 3

The dependence of the V_{oc}, V_{mp}, V_{mp}/V_{oc}, and two prediction performance indices for the PV arrays on different temperatures under irradiation intensity of 1000 W/m^2. The test results were experimentally measured and estimated by the direct-prediction method, respectively.

Temperature (°C)	Experimental results			Direct-prediction method		Prediction performance indices	
	V_{oc} (V)	V_{mp} (V)	V_{mp}/V_{oc}	V_{mp} (V)	V_{mp}/V_{oc}[a]	Prediction error: ΔV_{mp} (V)	% Prediction error: V_{mp}/V_{oc}
0	39.774	32.394	0.8145	32.549	0.8183	0.155	0.48
25	36.828	29.991	0.8144	30.015	0.8150	0.024	0.08
50	33.882	27.571	0.8137	27.309	0.8060	−0.262	−0.95
75	30.936	25.161	0.8133	24.925	0.8057	−0.236	−0.94

[a] The values of open-circuit voltage (V_{oc}) used are the same as the experimental ones.

In addition, the increase in the minority-carrier diffusion length has a positive impact on the photocurrent I_g. Not only does the short-circuit current I_{sc} rise from 7.779 to 8.256 A, the I_{mp}/I_{sc} also increases from 0.9294 to 0.9363 A, due to the increase in the temperature. Using the proposed direct-prediction method we obtain the average values of the prediction error in ΔI_{mp} and the percentage prediction error in I_{mp}/I_{sc} (%) between the actual and estimated maximum power currents, which are 0.039 A and 0.52%, respectively. The results indicate that the proposed method can achieve an accurate estimation of the MPP of PV arrays under environment variations such as temperature. Comparing the calculated results with the experimental results in Fig. 7 we can clearly see that they are pretty much alike. As temperature increases, the degradation in the softness on the knee of the *P–I* curve will also reduce the impact of the fill factor [25]. The overall effect of this causes a reduction in efficiency as temperature rises.

Fig. 8 shows the variation curves of ratios V_{mp}/V_{oc} and I_{mp}/I_{sc} estimated from the *P–I* characteristic curve of PV arrays under different temperatures and at an irradiation intensity of 1000 W/m^2. The V_{oc} and V_{mp} of the PV arrays both linearly decrease with the increase in temperature. The temperature coefficient of V_{mp}/V_{oc} is $-0.036\%/^\circ$C. On the other hand, both I_{sc} and I_{mp} increase slightly with temperature. The temperature coefficient of I_{mp}/I_{sc} is 0.034%/$^\circ$C. The tendency of the Si-based PV modules is the same [35]; however, the temperature coefficients are about half those of the general single-crystalline Si-based PV modules. Moreover, it can also be seen in the inset to Fig. 8
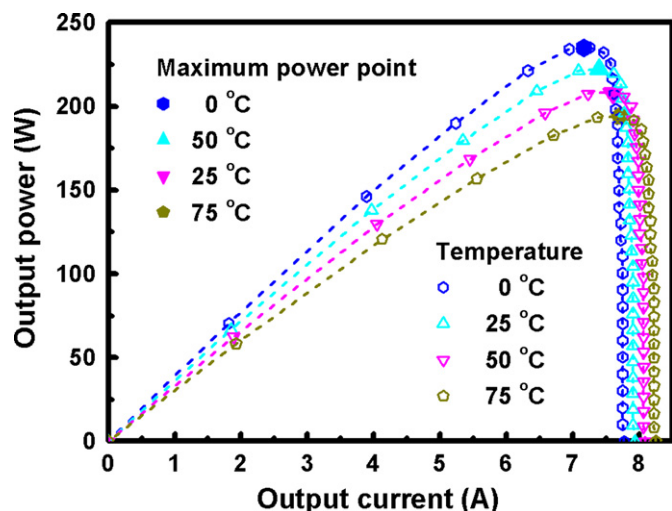
that the linear proportionality relationship between the short-circuit current I_{sc} and the current I_{mp} of the MPP is constant and equal to 0.936. This result is quite close but more accurate than the empirically predicted value of 0.9, even if the temperature is changed. This is because the short-circuit current is almost the same as the photo-current generated from irradiation, and the current I_{mp} of the MPP is proportional to the irradiation.

In general, the MPPT of PV arrays must be performed under various weather conditions. The proposed MPP prediction method can be used to develop control rules for MPPT control for PV arrays.

5. Conclusions

A new, simple, accurate, and low calculation burden method for estimating the MPP of PV arrays is presented. In this study, we investigate the effectiveness of the proposed direct-prediction MPP method for PV arrays subject to different irradiation intensities and temperatures. Based on the p–n junction recombination mechanism, we are able to simply estimate the MPP of PV arrays with our prediction method, to ensure that the maximum utilization efficiency and maximum power output of PV arrays can be achieved in practical applications. Our experiments demonstrate that changes in temperature mainly affect the PV output voltage, while changes in irradiation influence the PV output current. Both the output power and the evolution of the characteristic ratios V_{mp}/V_{oc} and I_{mp}/I_{sc} expressed as functions of irradiation intensity and temperature are found to be in good agreement with the theoretical method. The linear proportionality relationship between the
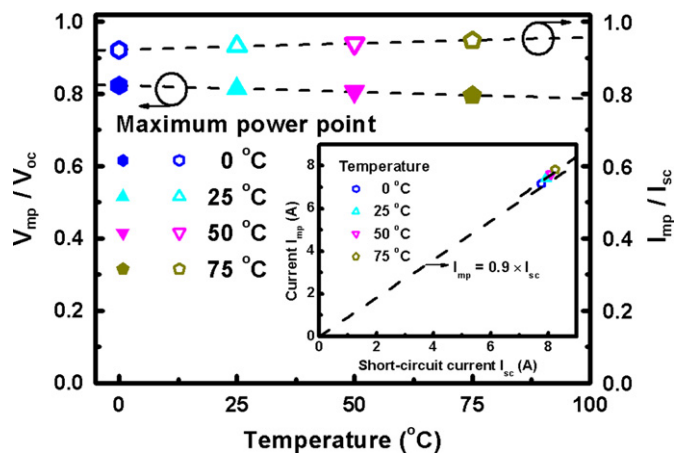

Fig. 7. The experimental and calculated *P–I* characteristics curves of the PV arrays under different temperatures and an irradiation intensity of 1000 W/m^2. The hollow symbols and dash lines in figure indicate the experimental and calculated *P–I* characteristics curves of the PV arrays, respectively. The labeled solid symbols indicate the MPPs of the PV arrays with different temperatures estimated by the direct-prediction method.

Fig. 8. The characteristic ratios of V_{mp}/V_{oc} and I_{mp}/I_{sc} estimated from the *P–I* characteristic curve of the PV arrays under different temperatures and an irradiation intensity of 1000 W/m^2. The inset shows the relationship between the short-circuit current I_{sc} and the current I_{mp} at the MPP for the PV arrays under different temperatures and an irradiation intensity of 1000 W/m^2.

Table 4
The dependence of the I_{sc}, I_{mp}, I_{mp}/I_{sc}, and two prediction performance indices for the PV arrays on different temperatures under irradiation intensity of 1000 W/m^2. The test results were experimentally measured and estimated by the direct-prediction method, respectively.

Temperature (°C)	Experimental results			Direct-prediction method		Prediction performance indices	
	I_{sc} (A)	I_{mp} (A)	I_{mp}/I_{sc}	I_{mp} (A)	I_{mp}/I_{sc}[a]	Prediction error: ΔI_{mp} (A)	% Prediction error: I_{mp}/I_{sc}
0	7.779	7.230	0.9294	7.175	0.9224	−0.055	−0.76
25	7.938	7.409	0.9334	7.402	0.9325	−0.007	−0.09
50	8.097	7.571	0.9350	7.608	0.9396	0.037	0.49
75	8.256	7.730	0.9363	7.788	0.9433	0.058	0.75

[a] The values of short-circuit current (I_{sc}) used are the same as the experimental ones.

short-circuit current and the current of the MPP echoes with the experimentally predicted values but are more accurate. This holds true even if the irradiation intensity or temperature changes. The effectiveness of the proposed method is verified through experiments carried out under various weather conditions and can also be applied to the method of MPPT and PV stability in future.

Acknowledgments

References

[1] X. Pelet, D. Favrat, G. Leyland, Multiobjective optimisation of integrated energy systems for remote communities considering economics and CO_2 emissions, Int. J. Therm. Sci. 44 (2005) 1180–1189.

[2] L. Gustavsson, P. Börjesson, B. Johansson, P. Svenningsson, Reducing CO_2 emissions by substituting biomass for fossil fuels, Energy 20 (1995) 1097–1113.

[3] M. Münster, H. Lund, Use of waste for heat, electricity, and transport—challenges when performing energy system analysis, Energy 34 (2009) 636–644.

[4] M. Beccali, P. Finocchiaro, B. Nocke, Energy and economic assessment of desiccant cooling systems coupled with single glazed air and hybrid PV/thermal solar collectors for applications in hot and humid climate, Sol. Energy 83 (2009) 1828–1846.

[5] K. Sakaki, K. Yamada, CO_2 mitigation by new energy systems, Energy Conver. Manage. 38 (1997) S655–S660.

[6] K. Yamada, H. Komiyama, K. Kato, A. Inaba, Evaluation of photovoltaic energy systems in terms of economics, energy, and CO_2 emissions, Energy Conver. Manage. 36 (1995) 819–822.

[7] P. Nema, R.K. Nema, S. Rangnekar, Minimization of green house gases emission by using hybrid energy system for telephony base station site application, Renew. Sust. Energ. Rev. 14 (2010) 1635–1639.

[8] P.K. Katti, M.K. Khedkar, Alternative energy facilities based on site matching and generation unit sizing for remote area power supply, Renew. Energy 32 (2007) 1346–1366.

[9] P.A. Østergaard, Reviewing optimisation criteria for energy systems analyses of renewable energy integration, Energy 34 (2009) 1236–1245.

[10] O. Ekren, B.Y. Ekren, Size optimization of a PV/wind hybrid energy conversion system with battery storage using simulated annealing, Appl. Energy 87 (2010) 592–598.

[11] M. Santarelli, M. Calì, S. Macagno, Design and analysis of stand-alone hydrogen energy systems with different renewable sources, Int. J. Hydrog. Energy 29 (2004) 1571–1586.

[12] B.S. Borowy, Z.M. Salameh, Methodology for optimally sizing the combination of a battery bank and PV array in a wind/PV hybrid system, IEEE Trans. Energy Convers. 11 (1996) 367–375.

[13] H.S. Rauschenbach, Solar cell array design handbook: The Principles and Technology of Photovoltaic Energy Conversion, Van Nostrand Reinhold Co., New York, 1980.

[14] K. Takigawa, N. Okada, N. Kuwabara, A. Kitamura, F. Yamamoto, Development and performance test of smart power conditioner for value-added PV application, Sol. Energy Mater. Sol. Cells 75 (2003) 547–555.

[15] S. Sopitpan, P. Changmuang, S. Panyakeow, Monitoring and data analysis of a PV system connected to a grid for home applications, Sol. Energy Mater. Sol. Cells 67 (2001) 481–490.

[16] J. Close, J. Ip, K.H. Lam, Water recycling with PV-powered UV-LED disinfection, Renew. Energy 31 (2006) 1657–1664.

[17] T. Hiyama, S. Kouzuma, T. Imakubo, Identification of optimal operating point of PV modules using neural network for real time maximum power tracking control, IEEE Trans. Energy Convers. 10 (1995) 360–367.

[18] T. Hiyama, K. Kitabayashi, Neural network based estimation of maximum power generation from PV module using environmental information, IEEE Trans. Energy Convers. 12 (1997) 241–247.

[19] C.R. Sullivan, M.J. Powers, A high-efficiency maximum power point tracker for photovoltaic arrays in a solar-powered race vehicle, in: Proceedings of the IEEE Power Electronics Specialists Conference, 20–24 June 1993, Seattle, WA, USA, pp. 574–580.

[20] J.A. Gow, C.D. Manning, Controller arrangement for boost converter systems sourced from solar photovoltaic arrays or other maximum power sources, in: Proceedings of the Institution of Electrical Engineers—Electric Power Applications vol. 147, 2000, pp. 15–20.

[21] J.H.R. Enslin, M.S. Wolf, D.B. Snyman, W. Sweigers, Integrated photovoltaic maximum power point tracking converter, IEEE Trans. Ind. Electron. 44 (1997) 769–773.

[22] J.J. Shoeman, J.D. van Wyk, A simplified maximal power controller for terrestrial photovoltaic panel arrays, in: Proceedings of the IEEE Power Electronics Specialists Conference, 14–17 June 1982, Cambridge, MA, USA, pp. 361–367.

[23] O. Wasynzczuk, Dynamic behavior of a class of photovoltaic power systems, IEEE Trans. Power Appl. Syst. PAS-102 (1983) 3031–3037.

[24] K.H. Hussein, I. Muta, T. Hoshino, M. Osakada, Maximum photovoltaic power tracking: An algorithm for rapidly changing atmosphere conditions, in: Proceedings of the Institution of Electrical Engineers—Generation, Transmission, and Distribution, vol. 142, 1995, pp. 59–64.

[25] S.M. Sze, Physics of semiconductor devices, second ed., Wiley, New York, 1981.

[26] B.K. Bose, P.M. Szczeny, R.L. Steigerwald, Microcomputer control of a residential photovoltaic power conditioning system, IEEE Trans. Ind. Appl. IA-21 (1985) 1182–1191.

[27] C.C. Hua, J.R. Lin, C.M. Shen, Implementation of a DSP-controlled photovoltaic system with peak power tracking, IEEE Trans. Ind. Electron. 45 (1998) 99–107.

[28] M. Bashahu, A. Habyarimana, Review and test of method for determination of the solar cell series resistance, Renew. Energy 6 (1995) 129–138.

[29] J. Thongpron, K. Kirtikara, C. Jivacate, A method for the determination of dynamic resistance of photovoltaic modules under illumination, Sol. Energy Mater. Sol. Cells 90 (2006) 3078–3084.

[30] M.K. El-Adawi, I.A. Al-Nuaim, A method to determine the solar cell series resistance from a single $I–V$. Characteristic curve considering its shunt resistance—new approach, Vacuum 64 (2001) 33–36.

[31] J.M. Kwon, K.H. Nam, B.H. Kwon, Photovoltaic power conditioning system with line connection, IEEE Trans. Ind. Electron. 53 (2006) 1048–1054.

[32] V.V.R. Scarpa, S. Buso, G. Spiazzi, Low-complexity MPPT technique exploiting the PV Module MPP locus characterization, IEEE Trans. Ind. Electron. 56 (2009) 1531–1538.

[33] N. Mutoh, M. Ohno, T. Inoue, A method for MPPT control while searching for parameters corresponding to weather conditions for PV generation systems, IEEE Trans. Ind. Electron. 53 (2006) 1055–1065.

[34] C. Carrero, J. Rodríguez, D. Ramírez, C. Platero, Simple estimation of PV modules loss resistances for low error modelling, Renew. Energy 35 (2010) 1103–1108.

[35] D.L. King, J.A. Kratochvil, W.E. Boyson, Temperature coefficients for PV modules and arrays: measurement methods, difficulties, and results, in: Proceedings of the IEEE Photovoltaic Specialists Conference, 29 September–03 October 1997, Anaheim, CA, USA, pp. 1183–1186.